BBA - Molecular Cell Research 1871 (2024) 119621

Contents lists available at ScienceDirect

BBA - Molecular Cell Research

journal homepage: www.elsevier.com/locate/bbamcr

Research paper

Disorders in the CMG helicase complex increase the proliferative capacity and delay chronological aging of budding yeast

Karolina Stępień [a], Adrianna Skoneczna [b,*], Monika Kula-Maximenko [c], Łukasz Jurczyk [d], Mateusz Mołoń [e,*]

[a] Institute of Medical Sciences, Rzeszów University, 35-959 Rzeszów, Poland
[b] Institute of Biochemistry and Biophysics, Polish Academy of Sciences, 02-106 Warsaw, Poland
[c] The Franciszek Górski Institute of Plant Physiology, Polish Academy of Sciences, 30-239 Krakow, Poland
[d] Institute of Agricultural Sciences, Rzeszów University, 35-601 Rzeszów, Poland
[e] Institute of Biology, Rzeszów University, 35-601 Rzeszów, Poland

ARTICLE INFO

Keywords:
Aging
Cell cycle
CDC45
CMG helicase
GINS complex
MCM complex

ABSTRACT

The replication of DNA requires specialized and intricate machinery. This machinery is known as a replisome and is highly evolutionarily conserved, from simple unicellular organisms such as yeast to human cells. The replisome comprises multiple protein complexes responsible for various steps in the replication process. One crucial component of the replisome is the Cdc45-MCM-GINS (CMG) helicase complex, which unwinds double-stranded DNA and coordinates the assembly and function of other replisome components, including DNA polymerases. The genes encoding the CMG helicase components are essential for initiating DNA replication. In this study, we aimed to investigate how the absence of one copy of the CMG complex genes in heterozygous *Saccharomyces cerevisiae* cells impacts the cells' physiology and aging. Our data revealed that these cells exhibited a significant reduction in transcript levels for the respective CMG helicase complex proteins, as well as disruptions in the cell cycle, extended doubling times, and alterations in their biochemical profile. Notably, this study provided the first demonstration that cells heterozygous for genes encoding subunits of the CMG helicase exhibited a significantly increased reproductive potential and delayed chronological aging. Additionally, we observed a noteworthy correlation between RNA and polysaccharide levels in yeast and their reproductive potential, as well as a correlation between fatty acid levels and cell doubling times. Our findings also shed new light on the potential utility of yeast in investigating potential therapeutic targets for cancer treatment.

1. Introduction

The process of chromosomal DNA replication is conserved across all eukaryotes. DNA replication is a complex process that involves multiple proteins to ensure its accuracy. A highly regulated and coordinated collaboration among DNA replication factors is required for the precise and efficient duplication of genetic information. The DNA replication machinery plays a pivotal role in cell proliferation. One of the essential replication enzymes is DNA helicase, an enzyme responsible for unwinding double-stranded DNA before replicon assembly [1]. The replication helicase consists of three components: the catalytic core, which is the heterohexameric Mcm2-Mcm7 minichromosome maintenance (MCM) complex; the tetrameric Psf1-Psf2-Psf3-Sld5 (GINS) complex, which forms accessory proteins; and the Cdc45 protein, which serves as the DNA replication initiation factor. Together, these components form the CMG (Cdc45, MCM, GINS) helicase complex [2,3]. Given that the replication machinery is comprised of a variety of proteins and regulatory factors, any malfunction in these proteins can lead to a reduction in replication efficiency, resulting in replication stress. Replication stress caused by imbalances in replication factors makes cells more susceptible to damage. For instance, both excessive CMG helicase activity and delays in its functioning can lead to DNA damage. Excessive activity exposes single-stranded DNA regions to damaging factors, while delays create DNA strand tension that may result in DNA breakage and, ultimately, cell death [4–6]. Therefore, disrupting the replication machinery or its dysregulation could be used as a strategy for creating drugs that induce replication stress, particularly in cancer cells [7]. Additionally, inhibiting helicase activity in pathogens could prove crucial in

* Corresponding authors.
E-mail addresses: ada@ibb.waw.pl (A. Skoneczna), mmolon@ur.edu.pl (M. Mołoń).

https://doi.org/10.1016/j.bbamcr.2023.119621
Received 10 May 2023; Received in revised form 8 October 2023; Accepted 22 October 2023
Available online 29 October 2023

the fight against various infectious diseases. Overall, helicase has become an attractive therapeutic target for the treatment of bacterial and viral infections, autoimmune disorders, and cancers. Proteins associated with the CMG helicase complex are vital for cell cycle progression, as well as for both the initiation and elongation steps during DNA replication. However, it remains unclear whether disturbances in pre-replication complex formation affect cell physiology and aging. In eukaryotes, the pre-replication complex typically consists of six subunits of the ORC complex (Orc1-Orc6), Cdc6, Cdt1, and a heterohexameric MCM complex (Mcm2-Mcm7). Recent research has shown that reduced expression of *ORC1-ORC6* genes, which encode subunits of the origin recognition complex (ORC), significantly extends both budding and average chronological lifespans. The ORC complex is yet another replication initiation factor that initiates DNA replication in eukaryotes by binding to DNA replication origins [8].

Aging is a complex process characterized by the loss of the ability to reattain homeostasis following stress, ultimately leading to increased mortality and morbidity. It is also defined as a progressive decline in physiological integrity accompanied by decreasing fertility and an increased risk of mortality with age [9,10]. Two primary approaches are employed to study yeast aging. Replicative lifespan is defined as the number of buds produced before cell death. It has been suggested that yeast replicative aging is analogous to aging observed in stem cells of higher eukaryotes [11]. A cell's chronological lifespan is determined based on the time it survives in a non-budding state, and survival is measured by its ability to form colonies (in a stationary phase culture, survival decreases over time). Chronological aging in yeast is akin to aging in non-dividing cells [12]. Despite extensive research on this topic, the links between replication initiation and aging remain largely unknown.

Our study aims to investigate the impact of a reduction in the copy number of genes encoding the subunits of the CMG complex on diploid cell proliferation, their cell cycle, aging, and biochemical profile. The strong amino acid sequence homology between yeast and human components of CMG complexes suggests the potential extrapolation of our findings to human cells. Our results demonstrate that a decrease in the mRNA levels of any of the CMG helicase subunits leads to a significant increase in budding lifespan and delays the average chronological aging, likely attributable to a cell cycle delay. Additionally, we have reaffirmed previous findings regarding the reduction in DNA content during the chronological aging of diploid cells. Using Raman spectrometry techniques, we have also established a robust negative correlation between the level of polysaccharides and cell reproductive potential, as well as a strong correlation between cell doubling time and fatty acid levels.

2. Materials and methods

2.1. Strains and growth conditions

All yeast strains used in this study are listed in Table 1.

Yeast cells were cultured in a standard rich liquid YPD medium (1 % Difco Yeast Extract, 1 % Yeast Bacto-Peptone, 2 % (w/v) glucose) using a rotary shaker set at 150 rpm or on solid YPD medium containing 2 % agar. The experiments were conducted at a temperature of 28 °C.

For the CLS assay, the SDC medium was employed, which consisted of 0.67 % Bacto-yeast nitrogen base (without amino acids) and 2 % (*w/v*) glucose. It was further supplemented with L-histidine (60 mg/L), L-leucine (180 mg/L), and uracil (60 mg/L).

2.2. Growth rate determination

The growth assays were conducted in a liquid medium. Yeast cell suspensions were incubated at 28 °C for 12 h with continuous shaking (using a Heidolph Incubator 1000 at 1200 rpm). Growth was assessed by measuring the absorbance at 600 nm using an Anthos 2010 type 17,550 microplate reader at 2-h intervals over a 12-h period. In the second approach, cell counts per mL were determined for each culture using a Malassez chamber (Carl Roth, Lauda-Konigshofen, Germany).

Table 1
Strains used in this study.

Strain	Genotype	Source
BY4743 a/α	*Mat a/α; his3Δ1/his3Δ1; leu2Δ0/leu2Δ0; lys2Δ0/LYS2; MET15/met15Δ0; ura3Δ0/ura3Δ0*	Open Biosystems
CDC45/cdc45Δ	*Mat a/α; his3Δ1/his3Δ1; leu2Δ0/leu2Δ0; lys2Δ0/LYS2; MET15/met15Δ0; ura3Δ0/ura3Δ0; ylr103c::kanMX4/YLR103c*	Open Biosystems
MCM2/mcm2Δ	*Mat a/α; his3Δ1/his3Δ1; leu2Δ0/leu2Δ0; lys2Δ0/LYS2; MET15/met15Δ0; ura3Δ0/ura3Δ0; ybl023c::kanMX4/YBL023c*	Open Biosystems
MCM3/mcm3Δ	*Mat a/α; his3Δ1/his3Δ1; leu2Δ0/leu2Δ0; lys2Δ0/LYS2; MET15/met15Δ0; ura3Δ0/ura3Δ0; yel032w::kanMX4/YEL032w*	Open Biosystems
MCM4/mcm4Δ	*Mat a/α; his3Δ1/his3D1; leu2Δ0/leu2Δ0; lys2Δ0/LYS2; MET15/met15Δ0; ura3Δ0/ura3Δ0; ypr019w::kanMX4/YPR019w*	Open Biosystems
MCM5/mcm5Δ	*Mat a/α; his3Δ1/his3Δ1; leu2Δ0/leu2Δ0; lys2Δ0/LYS2; MET15/met15Δ0; ura3Δ0/ura3Δ0; ylr274w::kanMX4/YLR274w*	Open Biosystems
MCM6/mcm6Δ	*Mat a/α; his3Δ1/his3Δ1; leu2Δ0/leu2Δ0; lys2Δ0/LYS2; MET15/met15Δ0; ura3Δ0/ura3Δ0; ygl201c::kanMX4/YGL201c*	Open Biosystems
MCM7/mcm7Δ	*Mat a/α; his3Δ1/his3Δ1; leu2Δ0/leu2Δ0; lys2Δ0/LYS2; MET15/met15Δ0; ura3Δ0/ura3Δ0; ybr202w::kanMX4/YBR202w*	Open Biosystems
PSF1/psf1Δ	*Mat a/α; his3Δ1/his3Δ1; leu2Δ0/leu2Δ0; lys2Δ0/LYS2; MET15/met15Δ0; ura3Δ0/ura3Δ0; ydr013w::kanMX4/YDR013w*	Open Biosystems
PSF2/psf2Δ	*Mat a/α; his3Δ1/his3Δ1; leu2Δ0/leu2Δ0; lys2Δ0/LYS2; MET15/met15Δ0; ura3Δ0/ura3Δ0; yjl072c::kanMX4/YJL072c*	Open Biosystems
PSF3/psf3Δ	*Mat a/α; his3Δ1/his3Δ1; leu2Δ0/leu2Δ0; lys2Δ0/LYS2; MET15/met15Δ0; ura3Δ0/ura3Δ0; yol146w::kanMX4/YOL146w*	Open Biosystems
SLD5/sld5Δ	*Mat a/α; his3Δ1/his3Δ1; leu2Δ0/leu2Δ0; lys2Δ0/LYS2; MET15/met15Δ0; ura3Δ0/ura3Δ0; ydr489w::kanMX4/YDR489w*	Open Biosystems
ndt80Δ/ndt80Δ	*Mat a/α; his3Δ1/his3Δ1; leu2Δ0/leu2Δ0; lys2Δ0/LYS2; MET15/met15Δ0; ura3Δ0/ura3Δ0; yhr124w::kanMX4/ yhr124w:: kanMX4*	Open Biosystems

2.3. Calculation of the mean doubling time

The mean doubling time was computed for each analyzed strain following the method outlined in a previous study [13]. Doubling times were calculated as part of the regular budding lifespan determination. To account for the initial delay and longer doubling times during the first two reproductive cycles on a new medium, we excluded these cycles from our calculations. A minimum of 90 cells were examined in two independent experiments, with 45 cells included in each experiment, and the results were reported as mean values with standard deviations (SD). Statistical significance was determined by a p-value of <0.001 using one-way ANOVA.

2.4. Measurement of cell metabolic activity

FUN-1 was employed to measure yeast metabolic activity following the manufacturer's instructions (Molecular Probes, Eugene, OR, USA), with minor modifications as detailed in [14]. The fluorescence of the cell suspension was assessed using a TECAN Infinite 200 microplate reader after a 15-min incubation at 28 °C in the dark (Grodig, Austria). Cell metabolic activity was quantified by calculating the change in the ratio of red to green fluorescence.

As per the protocol, the FUN1 stain permeates the cell and initially stains the cytoplasm with green fluorescence. Subsequent processing of the dye by live cells leads to the formation of red vacuolar structures, often taking on a stick-like shape, concurrent with a decrease in green

cytoplasmic fluorescence (deceased cells exhibit no red structures). The development of these intravacuolar structures necessitates both intact plasma membrane integrity and metabolic functionality. Mean values and standard deviations (SD) were computed from data obtained from at least five cultures for each strain.

2.5. Sporulation efficiency assay

Following pre-growth in rich YPD medium, diploid strains were cultivated for 14 days at 28 °C on sporulation medium, which consisted of 0.1 % yeast extract, 1 % potassium acetate, 0.05 % glucose, and 2 % agar, as previously outlined [15]. Subsequently, cells were resuspended in water. Both cells and asci were quantified using a cell-counting chamber (Malassez), with a minimum of 300 cells counted per sample.

The sporulation frequency was expressed as a percentage of the asci count relative to the total cell count, normalized to the wild-type (WT) strain. Mean values and standard deviations (SD) were computed from data collected from at least three cultures for each strain.

2.6. Flow cytometry analysis

Samples for cytometric analysis were prepared following the protocol outlined in the reference [15]. In brief, cells were harvested, washed with water, and subsequently fixed with chilled (−20 °C) 70 % ethanol (Polmos, Warsaw, Poland) for 2 h at room temperature. Following fixation, cells were washed with FACS buffer (0.2 M Tris-HCl, pH 7.4, Sigma-Aldrich, Burlington, MA, USA, and 20 mM EDTA, Merck, Darmstadt, Germany) and then incubated for 2 h at 37 °C in FACS buffer containing 1 mg per ml RNase A (Sigma-Aldrich, Burlington, MA, USA) to digest any RNA present in the samples. After another wash with phosphate-buffered saline (PBS), cells were stained with 100 μL of propidium iodide solution (50 μg per ml in PBS; Calbiochem, San Diego, CA, USA) overnight at 4 °C in the dark.

Subsequently, 900 μL of PBS was added, and the cells underwent three rounds of sonication, each lasting 10 s, in an ultrasonic bath (Branson 2800, Branson Ultrasonic Corporation, Danbury, CT, USA) before FACS analysis to assess DNA content. The analysis was carried out using a FACS Calibur analyzer (Becton-Dickinson, Franklin Lakes, NJ, USA), with a total of 10,000 cells counted in a single assay. At least three independent experiments were conducted for each strain and at selected time points during the CLS assay. Cells were analyzed with regard to DNA content and cell size, utilizing FL2 and FSC channels, respectively. The representative histograms are presented.

Cell cycle analysis was conducted on exponentially growing cells, utilizing two control strains - one haploid and one diploid - to facilitate the identification of cells in their respective cell cycle phases. The mean percentage of cells in the G1, S, and G2 phases of the cell cycle was determined based on data obtained from five independent biological replicates for each strain, including the wild-type (WT) control, with consideration given to the generation time. Standard deviations were also computed. To assess the statistical significance of differences between the CMG/cmg strain and the control in each cell cycle phase, a Student's *t*-test was employed.

2.7. Determination of budding lifespan

Cells were arranged on a YPD medium plate following an overnight growth period, employing a micromanipulator. The budding lifespan was assessed under microscopic examination, following the procedure outlined in reference [16]. The count of buds formed by each individual mother cell served as an indicator of its reproductive potential or budding lifespan. A minimum of 90 cells were meticulously examined across two independent experiments. The analysis was conducted utilizing a Nikon Eclipse E200 optical microscope (Nikon, Amsterdam, Netherlands) equipped with an attached micromanipulator.

2.8. Determination of the total lifespan

The total lifespan of a single mother yeast cell is defined as its duration of life, expressed in units of time. It is determined by summing the reproductive lifespan (the time between the first and last budding) and the post-reproductive lifespan (the time between the last budding and cell death). The assessment of the total lifespan in *S. cerevisiae* yeast followed the procedure described in [17], with slight modifications from [16]. Exponentially growing yeast cultures were sampled in 10-μl aliquots and transferred onto YPD plates with a solid medium containing Phloxine B (10 μg/mL). In each experimental run, 45 individual cells were subjected to analysis. Throughout the manipulation, the plates were maintained at 28 °C for 15 h and subsequently at 4 °C during the night. The results are based on measurements obtained from a minimum of 90 cells, which were analyzed in at least two independent experiments. The analysis was conducted via micromanipulation, utilizing a Nikon Eclipse E200 optical microscope equipped with a micromanipulator.

2.9. Chronological lifespan (CLS) assays

The chronological lifespan of cells incubated in a minimal medium (SDC) was determined following the method outlined in the reference [18]. In essence, yeast was cultured in an SDC medium supplemented with essential amino acids and 2 % (*w/v*) glucose. The assessment of chronological lifespan took place within the SDC medium, involving the measurement of cell viability at intervals of 2, 4, 7, 14, 21, and 28 days of cultivation. Propidium iodide staining was employed for quantitative survival assessment. The data presented here are the average values derived from a minimum of three independent experiments.

2.10. RNA isolation, reverse transcription and RT-qPCR

RNA extraction, reverse transcription, and RT-qPCR procedures were conducted following the methods previously outlined [8]. The primers employed for quantitative Real-Time PCR can be found in Table 2.

2.11. Raman spectroscopy

Raman spectroscopy was employed to analyze the chemical composition of yeast. The measurements were conducted using a Nicolet NXR 9650 FT-Raman Spectrometer equipped with an Nd:YAG laser (1064 nm) and an InGaAs detector. Samples of yeast were subjected to lyophilization prior to analysis. During the FT-Raman spectra measurements, the laser power was set at 0.5 W, with a laser beam diameter of 50 μm and a spectral resolution of 8 $cm^{-}1$. Spectra were recorded within the range of 250 to 1800 cm-1, representing an average of 64 scans. Subsequent processing of Raman spectra was carried out using the Omnic/Thermo Scientific software and OriginLab programs.

Principal Component Analysis (PCA) was employed to illustrate the correlation between the chemical composition and the yeast lines. PCA is a non-parametric technique used to extract information regarding similarities and differences among samples. These methods were applied within the Raman spectral ranges corresponding to polysaccharides, lipids, and RNA. The analysis and chart generation were conducted using OriginLab software.

2.12. Statistical analysis

The presented results are expressed as mean ± SD values obtained from all tested samples across two independent experiments. To assess differences between the WT and isogenic heterozygous diploid strains, one-way ANOVA and Dunnett's post hoc tests were employed. Statistical significance was considered when $p < 0.05$. The statistical analysis was carried out using Statistica 10.0 software, while statistical and multidimensional analysis for the Raman spectroscopy data was performed

Table 2
Primers used for RT-qPCR gene expression analysis.

Gene name	Forward Primer 5′- > 3’	Reverse Primer 5′- > 3’	Source
ACT1	AAGCTTTGTTCCATCCTTCT	GTACCACCGGACATAACG	*in this study*
CDC45	TAAATTGCTTGAACTGGACG	TCATCTTCGTCTTCTTCGTC	*in this study*
MCM2	GCAAAGACGAAGAAGGAGAA	ATTCCGAGTAACTGTTAGCC	*in this study*
MCM3	CTTGGAAGCTTTCGTTCAAA	GTGGACAGATCTGATAAGCT	*in this study*
MCM4	GTACCAACGTCAGTATCCAG	GTATAGTTCTTCGTCGGTAGT	*in this study*
MCM5	TTTGGATTCTGAACACGTCT	TGTTGTGTGTCTGCAATTTC	*in this study*
MCM6	CATGAGAGAAAATGGTGCTC	ACCTTCGGATCTCTTCAATG	*in this study*
MCM7	GGAGACTGAGGAATGAGAGA	TCAGTTTCATCCTCGACAAC	*in this study*
PSF1	TTTATCCGGCTCTTTAGTGC	ATCAGACTGCCTTACGAAAA	*in this study*
PSF2	GGTTCTTTGGATCGCTCTAT	CGGCAACTCACTAAACCTAT	*in this study*
PSF3	AGAACCTGTACCTTTTGTGG	TGGCTAGACTGAAGAAATGC	*in this study*
SLD5	GCCTATGCCTAACGAATCTA	ATTGGCGCAAATAAAGTGAG	*in this study*

using PAST 3.0 and Origin 2018 software.

3. Results

3.1. Heterozygosity in any gene encoding subunit of the CMG helicase in the diploid cell leads to growth rate disorders likely resulting from the delay in G1/S transition during the cell cycle

The CMG helicase is comprised of 11 proteins, specifically: Cdc45, Mcm2-Mcm7 (forming the MCM complex), Psf1-Psf3, and Sld5 (part of the GINS complex). Given the essential nature of these proteins for cell growth, our study employed heterozygous yeast strains in diploid organisms with respect to the genes encoding the CMG helicase subunits. For simplicity, we will refer to these strains as CMG/cmg strains. These strains were sourced from the yeast knockout collection (Table 1), with BY4743 serving as the control. These strains facilitated a series of experiments aimed at elucidating the role of the CMG helicase in chronological aging.

Firstly, we conducted a comparison of the growth rate and average doubling time of CMG/cmg strains on YPD medium containing 2 % glucose. Figs. 1a and b clearly demonstrate that nearly all of the analyzed strains exhibited a slower growth rate. To estimate the growth rate, we employed two different approaches: changes in optical density and changes in the number of cells per mL of culture. We have presented the results of both measurements because the analysis of doubling time revealed a statistically significant extension of the cell cycle, a phenomenon not observed in the growth rate analysis (Fig. 1a). This phenotype might be associated with alterations in various cellular characteristics, including cell size, transparency, granularity, and cell wall thickness among the analyzed strains. Consequently, we observed that all analyzed CMG/cmg strains exhibited cell cycle defects (Fig. 1b).

As demonstrated in Fig. 1c, the mean cell doubling time increased significantly for all assayed strains when compared to the wild type (WT). The calculation of the average doubling time of a single cell was performed during the budding lifespan analysis. This method represents the most precise means of estimating doubling time since it is applied to individual cells rather than the entire population. Several factors contribute to the estimation of doubling time-based on the growth curve, including the size of individual cells in the population and the initial doubling of virgin cells.

Next, we investigated whether sporulation efficiency was affected in the CMG/cmg strains. As depicted in Fig. 1d, nearly all the tested strains displayed altered sporulation efficiency; however, not all strains exhibited changes in the same direction. A significant reduction, approximately 90 %, in sporulation efficiency was observed exclusively in the *MCM2/mcm2Δ* strain. In contrast, the *MCM7/mcm7Δ* and *PSF2/psf2Δ* strains demonstrated an approximately 80 % increase in sporulation efficiency. For other strains, mild improvements in sporulation efficiency were noted, with the *CDC45/cdc45Δ* strain behaving identically to the WT. These data suggest that the copy number of genes encoding subunits of the CMG complex has an impact on meiosis.

Furthermore, it is worth noting that no more than two spores from each tetrad in any of the CMG/cmg strains were viable, confirming the essentiality of CMG helicase subunits (data not shown).

We also assessed whether the CMG/cmg strains exhibited differences from the WT strains in terms of other phenotypes. To evaluate yeast vitality, we employed FUN-1 staining, which measures the metabolic activity of the strains under examination. Cellular metabolic activity is indicated by a shift in the red ($\lambda = 575$ nm) to green ($\lambda = 535$ nm) fluorescence ratio. Higher red/green fluorescence ratios indicate increased metabolic activity in the cells. Most of the strains displayed a tendency toward higher metabolic activity compared to the WT. However, this tendency became statistically significant for the *MCM2/mcm2Δ* and *MCM4/mcm4Δ* strains ($p < 0.05$) and the *MCM7/mcm7Δ* and *PSF1/psf1Δ* strains ($p < 0.01$) (Fig. 1e).

Considering our anticipation of potential replication disruptions in the CMG/cmg strains due to potentially reduced levels of proteins involved in this process, we conducted a flow cytometry analysis of propidium iodide-stained cells to investigate any cell cycle abnormalities (Fig. 2a). When the generation times of the analyzed strains are similar, changes in the percentage of cells in a specific cell cycle phase in asynchronously growing cells are typically indicative of the duration of that phase. However, when generation times vary, these differences must be taken into account when analyzing the experimental data [19]. On average, the generation times of the tested strains differed by approximately 10 %, with the *MCM7/mcm7Δ* strain being the exception, displaying a 21 % longer generation time compared to the WT. We factored in these differences and calculated the mean number of cells in specific cell cycle phases for all tested strains relative to the WT.

In the asynchronous culture of exponentially growing yeast populations, most of the analyzed strains exhibited changes in the percentage of cells within various cell cycle phases (Fig. 2b). The most noticeable alteration was observed in the number of G1 phase cells, which accumulated in all strains except for *SLD5/sld5Δ* and *MCM3/mcm3Δ*. Additionally, the *CDC45/cdc45Δ* strain displayed an increased accumulation of S phase cells, while the *MCM7/mcm7Δ* strain showed a significant increase in the number of G2 phase cells.

To address the question regarding the expression levels of genes encoding CMG helicase components in heterozygous CMG/cmg strains, we conducted a real-time PCR analysis. The experiment revealed a noteworthy reduction ($p < 0.05$) in the expression of all the examined genes in comparison to the wild type (WT), as depicted in Fig. 3. The most significant decrease was observed in the genes responsible for encoding the GINS complex subunits and the *MCM2* gene, which exhibited a reduction of over 50 % when compared to the WT.

3.2. Reduced expression of genes encoding the CMG complex components prolongs the reproductive potential and chronological lifespan

The rate of cellular aging constitutes a pivotal determinant in assessing the physiological condition of cells. Consequently, we inquired whether the reproductive potential, total lifespan, and chronological

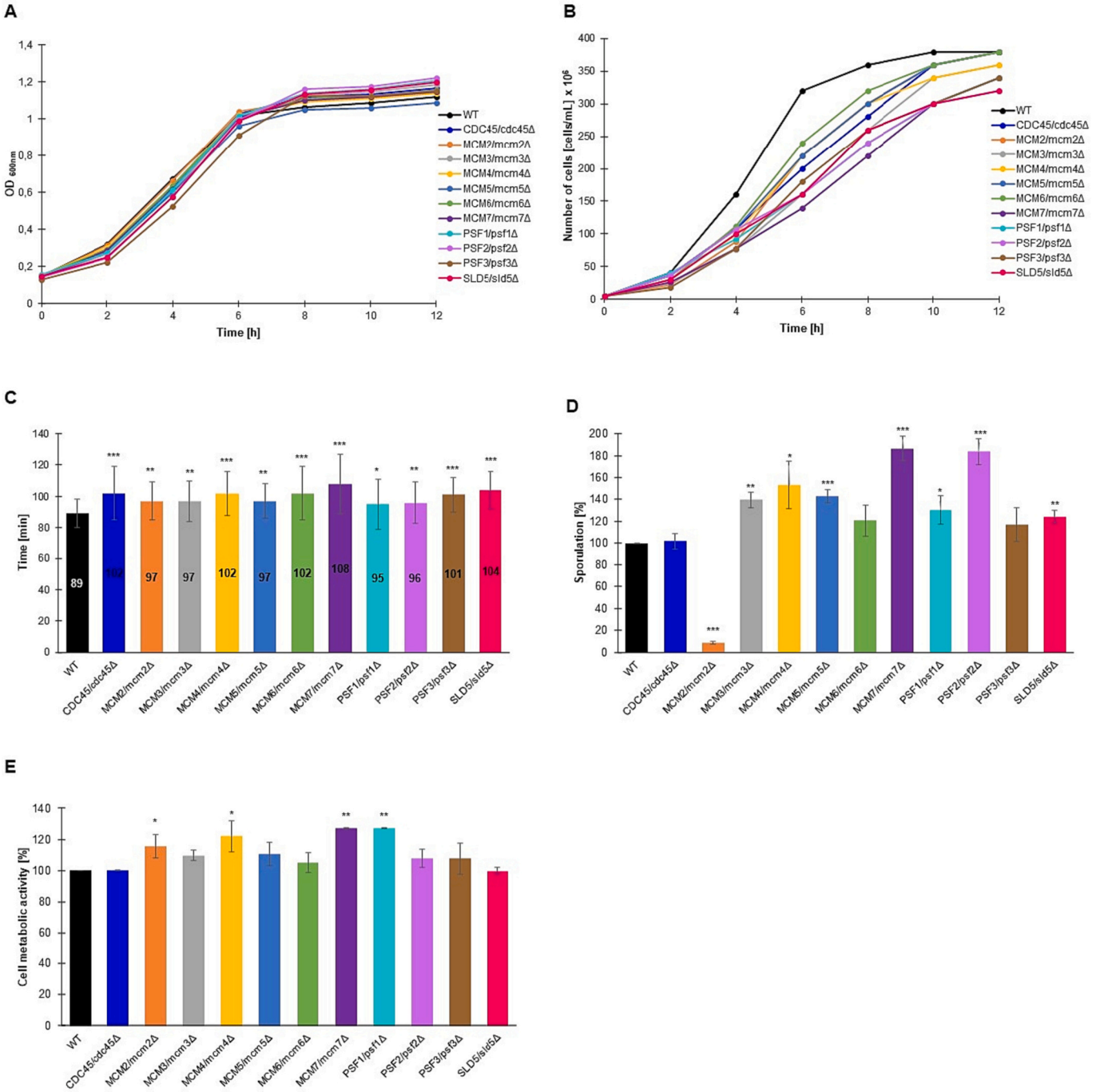

Fig. 1. Growth and metabolic phenotypes of heterozygous strains lacking one copy of the gene encoding a subunit of the CMG helicase. Comparison of growth curves for respective heterozygous strains and WT controls (BY4743). The density of the culture was determined by measuring the optical density at 600 nm (A) or the number of cells per mL (B). An average doubling time for the same strains as in (A) during the reproducing period. The error bars indicate standard deviations from two independent experiments (C). Sporulation frequency of the yeast strains heterozygous with respect to the CMG complex subunits encoding genes and the diploid control (BY4743) (D). Metabolic activity of the cells was estimated with FUN-1 stain for respective heterozygous strains and WT. Data are expressed as mean ± SD from three independent experiments. Bars indicate SD (E). Statistical significance was assessed using ANOVA and Dunnett's post hoc test (* $p < 0.05$; ** $p < 0.01$; *** $p < 0.001$) compared to WT.

aging were altered in the CMG/cmg strains. To gauge the age of mitotically active yeast cells, we employed the number of daughter cells produced by the mother cell, a conventional method. The total lifespan is the sum of the time a yeast cell spends reproducing and its post-daughter-production survival time.

To investigate the aging of mitotically active cells, we adopted a single-cell analysis approach. As illustrated in Fig. 4a, all the examined heterozygous strains displayed an enhanced capacity for reproduction compared to the wild type (WT). Only in the case of the *MCM2/mcm2Δ* heterozygous strain did the observed changes lack statistical significance. Remarkably, the *MCM3/mcm3Δ*, *MCM4/mcm4Δ*, *PSF3/psf3Δ*, and *SLD5/sld5Δ* strains exhibited the most substantial increases in reproductive potential, nearly 50 % higher than WT ($p < 0.001$). The data derived from the analysis of reproductive potential unequivocally demonstrate that the downregulation of genes encoding the CMG helicase components plays a pivotal role in cellular reproductive capacity.

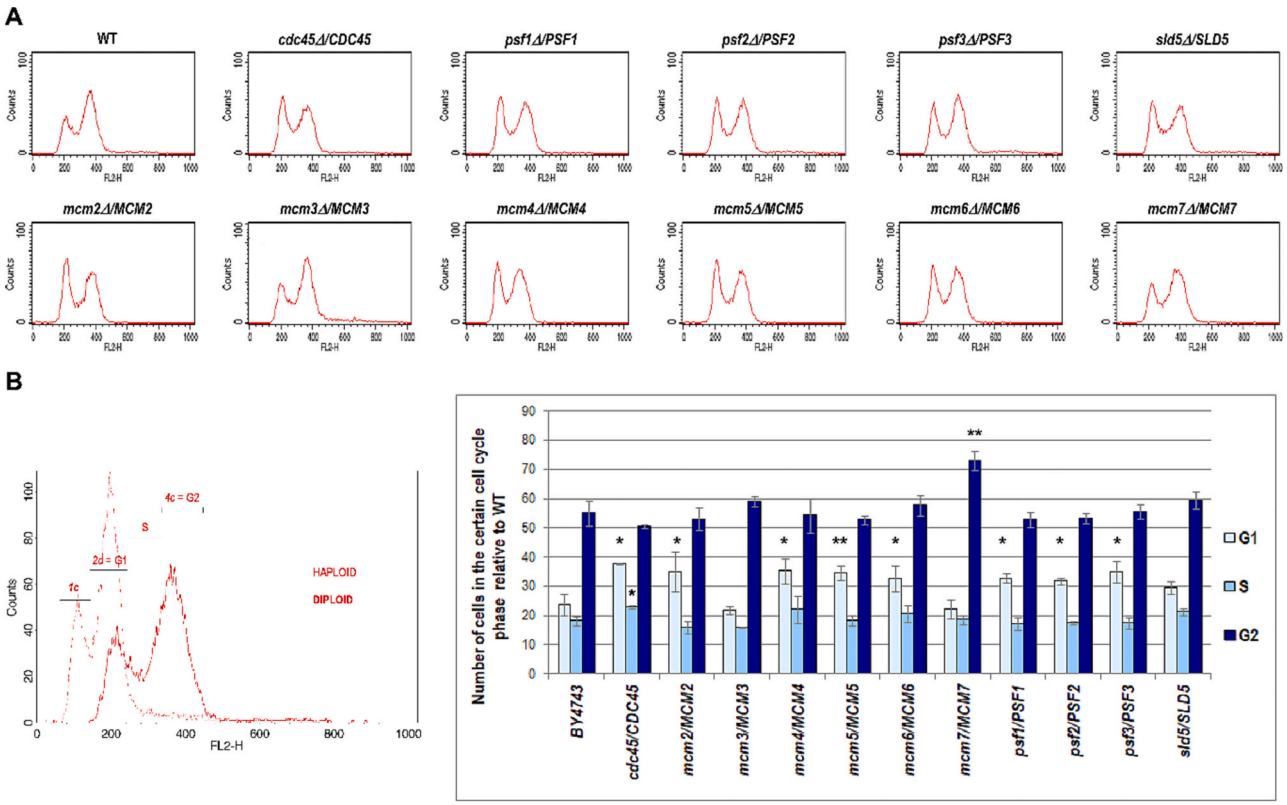

Fig. 2. Cells lacking one copy of the genes encoding subunits of the CMG helicase showed a slight delay in G1/S transition. (A) Flow cytometry analysis of the diploid WT strain (BY4743) and the isogenic heterozygous strains *CDC45/cdc45Δ*, *MCM2/mcm2Δ*, *MCM3/mcm3Δ*, *MCM4/mcm4Δ*, *MCM5/mcm5Δ*, *MCM6/mcm6Δ*, *MCM7/mcm7Δ*, *PSF1/psf1Δ*, *PSF2/psf2Δ*, *PSF3/psf3Δ*, and *SLD5/sld5Δ*. The representative histograms from three biological repetitions are presented. (B) Quantification of the cell cycle analysis. On the left, histograms for control strains, BY4741 (haploid) and BY4743 (diploid), with the gating conditions used to calculate the number of cells in the individual cell cycle phases. The graph on the right shows the quantification of the cell cycle analysis results. The percentage of cells in the specific cell cycle phase was calculated considering the strains' generation time and shown with respect to WT. The mean of five biological replicates is shown. Bars indicate standard deviations. Statistical significance with respect to the cell cycle phase of the WT control was assessed using Student's *t*-test (* p-val < 0.05; ** p-val < 0.01; *** p-val < 0.001).

As previously mentioned, we also ascertained the time parameters during replicative aging. Given the impact of reproductive potential, cell cycle irregularities, and increased doubling time (Fig. 1b) on reproductive lifespan, we anticipated that the studied CMG/cmg strains would exhibit an extended replicative lifespan (the duration of single-cell reproduction). Indeed, as depicted in Fig. 4b, all the scrutinized heterozygous strains displayed significantly prolonged replicative lifespans. However, for the *MCM2/mcm2Δ* strain, this extension lacked statistical significance.

Yeast cells don't undergo cell death immediately after reproduction; instead, they continue to exist for a specific duration known as the post-reproductive lifespan. As vividly illustrated in Fig. 4c, it becomes evident that the post-reproductive lifespans of the CMG/cmg strains experience a significant reduction. When assessing the post-reproductive lifespan, it's notable that the *MCM3/mcm3Δ* strain exhibited the briefest period following reproduction among all the strains tested. Conversely, the *MCM2/mcm2Δ* strain, which displayed a reproductive potential similar to that of the WT, demonstrated the longest post-reproduction lifespan.

We also determined the total lifespan of mitotically active cells. Interestingly, although there are no statistically significant differences in terms of total lifespan, it is slightly shorter on average compared to the control (Fig. 4d). Additionally, the results regarding the maximum survival time are quite intriguing. A notable difference was observed in the maximum survival time of heterozygous cells when compared to WT. As depicted in Fig. 4d, the WT strains exhibited the longest survival (297 h), followed by *MCM7/mcm7Δ* and *PSF3/psf3Δ* (262 h). In contrast, *MCM4/mcm4Δ* (147 h) and *PSF1/psf1Δ* (174 h) displayed shorter lifespans.

Lastly, we demonstrated a correlation between reproductive or post-reproductive lifespan and reproductive potential. The trend line in Fig. 5a reveals a strong positive correlation between the average reproductive lifespan and average reproductive potential, with a Pearson correlation coefficient of 0.955. Furthermore, we observed a negative correlation between post-reproductive lifespan and reproductive potential, with a Pearson correlation coefficient of −0.86 (Fig. 5b).

The second aging model employed in this study, referred to as the chronological aging model, enables us to assess the aging of post-mitotic cells within the analyzed population. One significant advantage of utilizing the CLS parameter is its ability to gauge the survival of non-budding cells, making it a suitable model for aging in post-mitotic mammalian cells, including humans. Monitoring CLS is a straightforward method that does not necessitate micromanipulation, as it relies on the cultivation of large populations of yeast cells, thereby facilitating longevity screening.

We employed two approaches for CLS analysis: fluorescent labeling of deceased cells and the conventional method of assessing survival by counting colony-forming units. As depicted in Fig. 6a and b, all CMG/cmg strains exhibited delayed senescence during the initial 14 days of the experiment, with the exception of *SLD5/sld5Δ*. Intriguingly, none of the strains were capable of forming colonies beyond the 21-day mark in the CLS experiment, whereas the WT strain remained viable. Approximately 15 % of cells within the WT strain population retained their viability, a statistically significant difference when compared to the CMG/cmg strains ($p < 0.001$) (Fig. 6a).

A standard microscopic analysis revealed a progressive increase in

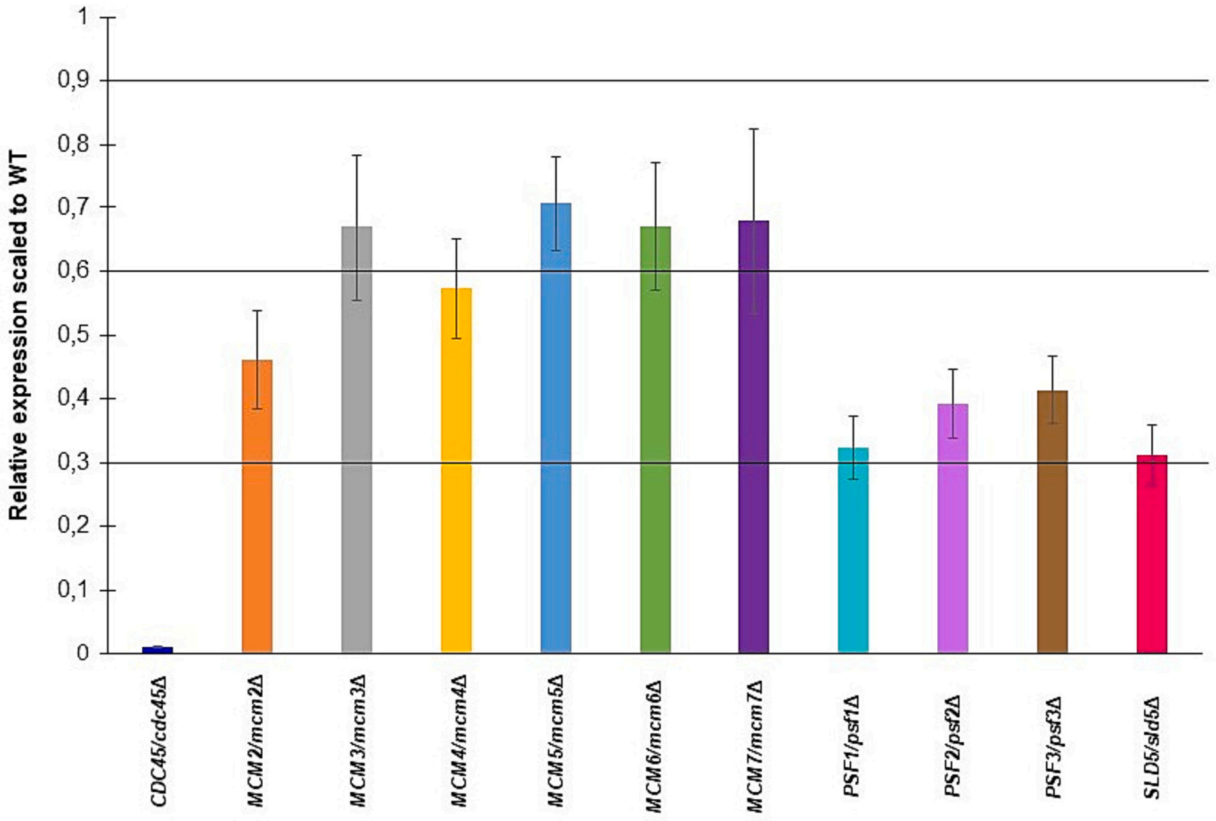

Fig. 3. Real-time-PCR analysis showed a decrease in the expression of genes encoding the CMG complex components in the respective CMG/cmg strains. The relative expression ratio of *CDC45*, *MCM2*, *MCM3*, *MCM4*, *MCM5*, *MCM6*, *PSF1*, *PSF2*, *PSF3*, *SLD5* normalized to *ACT1*, and to the expression level in WT in the *CDC45/cdc45Δ*, *MCM2/mcm2Δ*, *MCM3/mcm3Δ*, *MCM4/mcm4Δ*, *MCM5/mcm5Δ*, *MCM6/mcm6Δ*, *MCM7/mcm7Δ*, *PSF1/psf1Δ*, *PSF2/psf2Δ*, *PSF3/psf3Δ*, and *SLD5/sld5Δ* strains, respectively, was calculated from five independent repetitions. Standard deviation was also counted. All results were statistically significant, with $p < 0.05$.

cell size throughout the CLS experiment. To thoroughly assess the extent of this phenotype, we conducted a flow cytometry analysis. Our data clearly demonstrated a successive increase in cell size throughout the experiment, except for *MCM2/mcm2Δ* and *CDC45/cdc45Δ* strains, which exhibited larger cell sizes from the outset of the CLS experiment (Fig. 7). Notably, the smallest cells were observed at the experiment's commencement (2 days), while the largest ones were documented on days 14 and 21 of the study.

As cell size is known to positively correlate with ploidy, we also conducted tests to assess the DNA content of the cells, considering that replication stress can lead to abnormalities in DNA content. Remarkably, we observed a decline in viability and a reduction in ploidy levels over time in all CMG/cmg strains and the WT control (Fig. 7). This phenomenon mirrors findings reported recently in the chronological aging of diploid yeast cells with reduced expression of *ORC1- ORC6* genes, suggesting its widespread occurrence. One possible explanation for the emergence of haploid cells within the yeast population undergoing the chronological lifespan experiment is sporulation. To investigate this hypothesis, we employed the sporulation-deficient strain *ndt80Δ/ndt80Δ*. Ndt80 is a transcription factor crucial for the successful completion of meiosis and spore formation. Our CLS experiment, however, ruled out sporulation as the source of ploidy changes (refer to Supplementary data, Fig. 1). The intriguing phenomenon of ploidy reduction over time during the CLS experiment is further elaborated upon in a separate manuscript (currently in press [61]). Our data suggest potential connections between autophagy pathways and the decline in DNA content observed in chronological aging cells.

3.3. Decreased expression of the genes encoding the CMG helicase components causes a change in the biochemical fingerprint

The spectra for all analyzed CMG/cmg strains and the control (BY4743) are presented in Fig. 8, with marked peak positions (Raman shift) and their respective intensities. In the Raman spectra, peaks are observed in regions corresponding to proteins (850, 1004, 1035, 1280, 1453, 1610 cm-1), lipids (1254, 1662, 1775 cm^{-1}), polysaccharides (420, 520, 890, 960, 1090 cm-1), and RNA (400–800, 1330, 1390, 1575 cm^{-1}) [20–23].

Shifts in peak positions by a few nanometers or the emergence of additional peaks may signify alterations in the chemical composition and structure of these functional groups (Fig. 8). These variations in the Raman spectra may reflect differences in the metabolic activity of the examined yeast strains. Consequently, observable changes can be discerned in the bands specific to lipids, RNA, and polysaccharides within the provided Raman spectra.

The principal component analysis (PCA) demonstrates a positive correlation between the content of lipids and RNA, while it exhibits a strong negative correlation with the content of polysaccharides within the investigated yeast (Fig. 9). This analysis distinguishes six strains that exhibit distinct chemical compositions compared to other mutants: WT, *CDC45/cdc45Δ*, *MCM2/mcm2Δ*, *MCM4/mcm4Δ*, *MCM6/mcm6Δ*, and *PSF1/psf1Δ*. The polysaccharide content is high in the WT, *CDC45/cdc45Δ*, and *MCM2/mcm2Δ* strains and low in the *MCM4/mcm4Δ*, *MCM6/mcm6Δ*, and *PSF1/psf1Δ* strains. The *MCM2/mcm2Δ* strain is distinguished by the highest content of lipids and RNA, while the lowest content is found in the WT and *PSF1/psf1Δ* strains.

Next, we investigated the association between replicative aging parameters and the levels of lipids, polysaccharides, or RNA. As depicted in

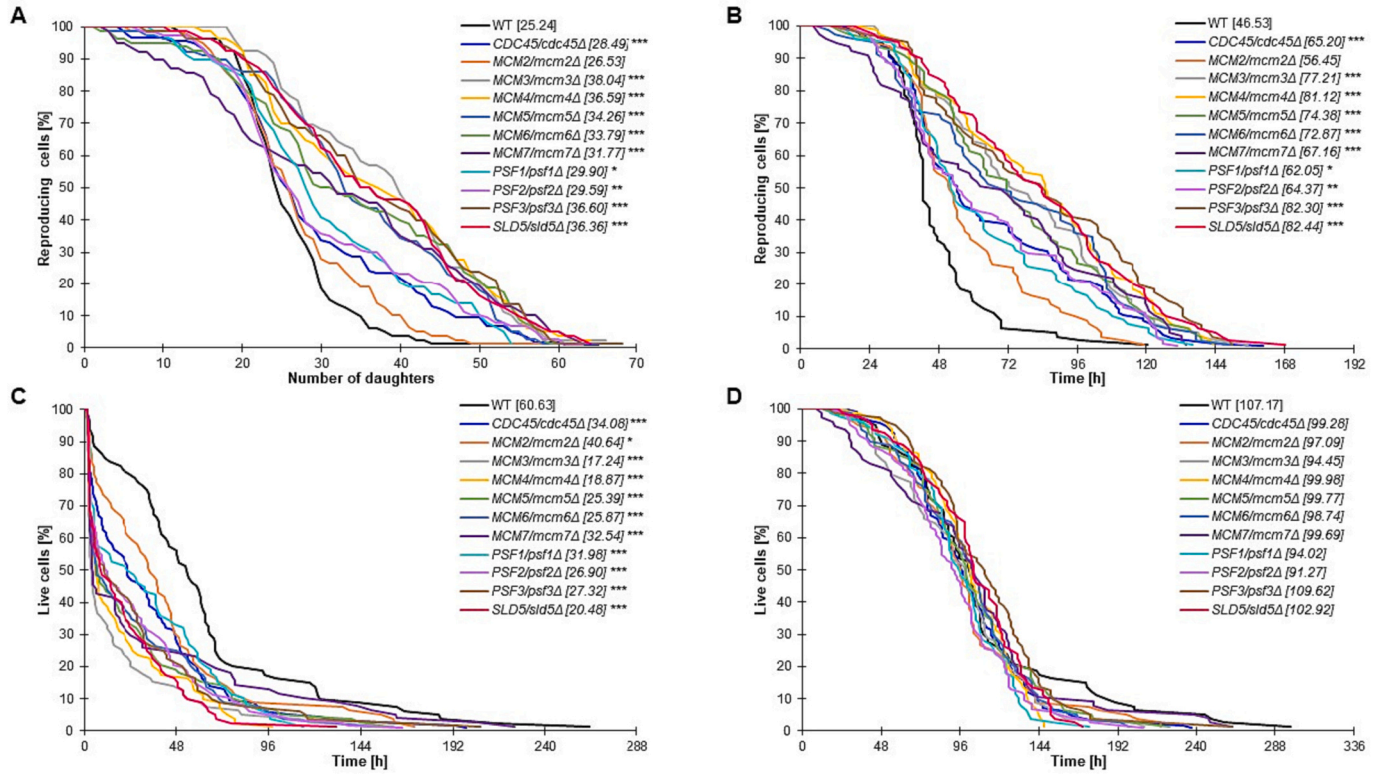

Fig. 4. Aging phenotypes of the cells with lowered expression of genes encoding the CMG complex subunits. Comparison of the reproductive potential (A), reproductive lifespan (B), post-reproductive lifespan (C) and total lifespan (D) of the diploid reference yeast strain BY4743 (WT) and isogenic heterozygous strains. Statistical significances were assessed using ANOVA and Dunnett's post hoc test (* $p < 0.05$, ** $p < 0.01$, *** $p < 0.001$). The mean value for a total of 90 cells from two independent experiments is shown in parentheses.

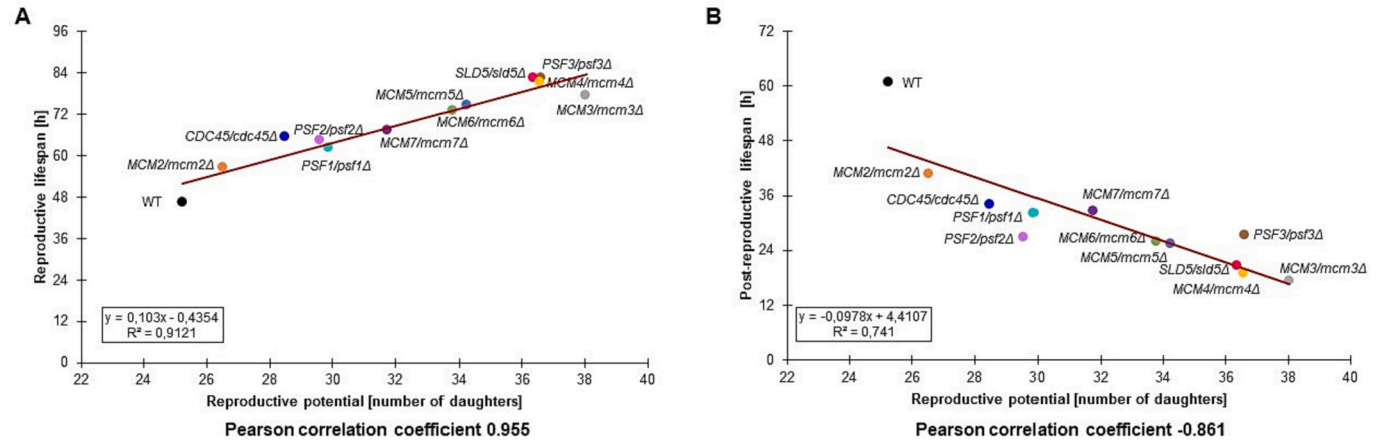

Fig. 5. Relationship between the average reproductive potential and average reproductive lifespan according to Pearson's correlation coefficient (A) and between the average reproductive potential and average post-reproductive lifespan (B) of the WT strain (BY4743) and the isogenic heterozygous CMG/cmg strains.

Fig. 10, a robust negative correlation exists between the levels of polysaccharides and reproductive potential (Fig. 10a), along with a moderate correlation between reproductive potential and RNA levels (Fig. 10b). Furthermore, our study marks the pioneering discovery of a substantial correlation between doubling time and elevated fatty acid levels (Fig. 10c).

In the final stage of our study, we conducted comprehensive metabolic analyses of the CMG/cmg strains under varying environmental conditions. Various metabolic conditions were employed to assess the phenotypes of the yeast mutants (Fig. 11). Notably, all strains displayed heightened resistance to cell wall stress induced by Calcofluor white and Congo red, as depicted in Fig. 11. Furthermore, the *CDC45/cdc45Δ* and *MCM7/mcm7Δ* cells were highly resistant to osmotic stress (treatment with 1 M NaCl), while *MCM2/mcm2Δ*, *MCM4/mcm4Δ*, *MCM6/mcm6Δ*, and *SLD5/sld5Δ* strains exhibited a greater sensitivity to osmotic stress than the WT control. Interestingly, we also found that the *MCM2/mcm2Δ* strain was sensitive to heat shock and genotoxic stress inducers such as zeocin and camptothecin.

4. Discussion

DNA replication is a fundamental and indispensable process within a cell, ensuring the accurate duplication of the genome (as reviewed in [24–27]).

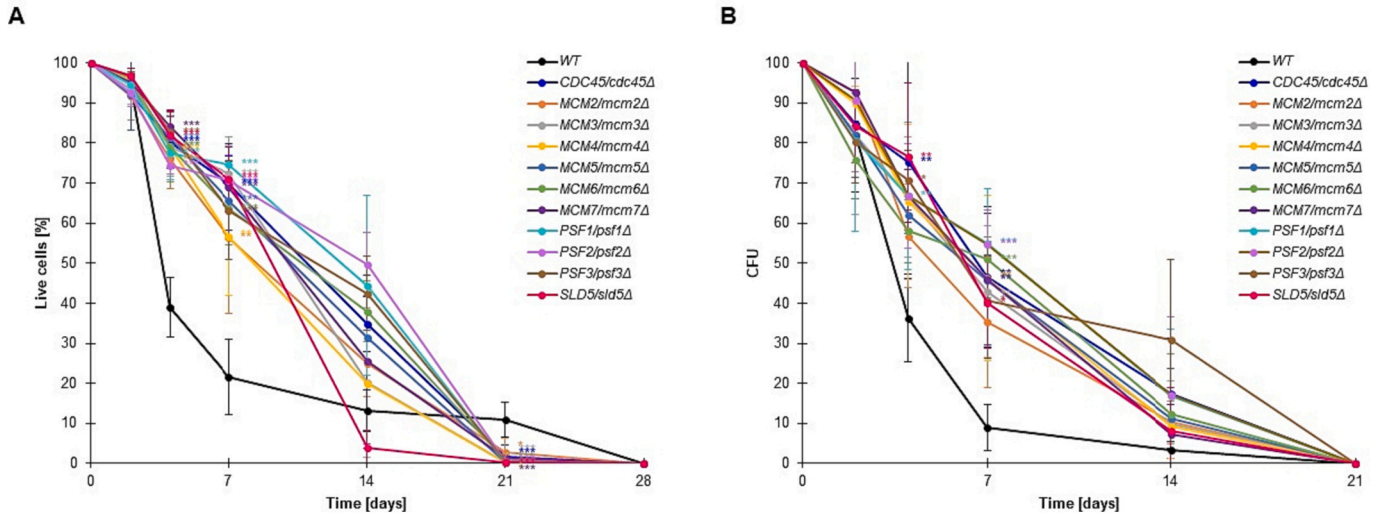

Fig. 6. The decreased expression of genes encoding the CMG helicase subunits determines yeast's chronological aging. Chronological lifespan of the diploid WT (BY4743) and the isogenic heterozygous strains *CDC45/cdc45Δ*, *MCM2/mcm2Δ*, *MCM3/mcm3Δ*, *MCM4/mcm4Δ*, *MCM5/mcm5Δ*, *MCM6/mcm6Δ*, *MCM7/mcm7Δ*, *PSF1/psf1Δ*, *PSF2/psf2Δ*, *PSF3/psf3Δ*, and *SLD5/sld5Δ*. Survival was determined by propidium iodide staining (A) and by the clonogenicity assay (expressed in colony-forming units, CFU) (B). Error bars represent standard deviations obtained from three independent experiments. Statistical significance was assessed using ANOVA and Dunnett's post hoc test (* $p < 0.05$, ** $p < 0.01$, *** $p < 0.001$).

In eukaryotes, the MCM complex, composed of six homologous Mcm2-Mcm7 proteins, forms a helicase ring. This complex becomes activated through the involvement of five auxiliary factors, namely Cdc45 and GINS tetramers, ultimately resulting in the formation of the 11-subunit CMG complex (Cdc45, MCM, GINS) [28]. The vital role of the GINS complex in maintaining replication fidelity in budding yeast has been extensively documented. Disruption of the GINS complex leads to an increase in the spontaneous mutation rate and instability in repetitive sequences [29,30]. The GINS complex plays a crucial role in the initiation of DNA replication, as it is part of transient protein complexes that assemble during the early stages of replication, preceding the formation of the active CMG helicase complex [31].

During the G/S transition, cyclin-dependent kinases (CDKs) and Dbf4-dependent kinases (DDK) activate the pre-replication complex (pre-RC), facilitating DNA unwinding [32]. Upon entering the S phase, both kinases play pivotal roles in promoting the assembly of replication forks. Additional pre-RC formation is inhibited, allowing for subsequent DNA polymerase loading and the initiation of bidirectional DNA replication.

It has been demonstrated that the S-phase checkpoint response can decelerate or halt fork progression, concurrently stabilizing the association of the MCM complex with the replication fork during DNA repair following DNA damage [33]. In our experiments, we observed that yeast cells with reduced expression of genes encoding CMG helicase subunits experienced alterations in their cell cycle. Most of the analyzed CMG/cmg strains exhibited a slight delay in G1/S transition. Notably, the *MCM7/mcm7Δ* and *MCM3/mcm3Δ* strains displayed an increased accumulation of cells in the G2 phase.

In our previous research, we demonstrated that heterozygous strains with decreased expression of genes encoding ORC complex subunits had significantly prolonged G1 phases in the cell cycle, resulting in a noteworthy increase in cell doubling time during subsequent budding [8]. A similar effect was anticipated for CMG/cmg strains, and our observations indeed confirmed this hypothesis. Interestingly, our results indicated that meiosis in CMG/cmg heterozygous strains was also affected. This finding holds significance when extrapolating these data to the context of gametogenesis in higher eukaryotes.

It has been demonstrated in human fibroblasts that the levels of Mcm2–Mcm7 proteins decrease in senescent cells [34,35]. We sought to determine whether a reduction in the expression of MCM complex subunits or other components of the CMG helicase would induce premature aging in a yeast aging model. Two primary approaches are commonly used to study yeast aging:

Replicative Lifespan: This refers to the number of buds produced by mother cells before their demise. Replicative lifespan is assessed at the single-cell level by counting the doublings performed by a mother cell, as its buds are removed individually through micromanipulation. This methodology takes advantage of the asymmetrical division of mother and daughter cells during budding. Therefore, yeast replicative aging mirrors the aging process in asymmetrically dividing cells, such as stem cells in higher eukaryotes.

Chronological Aging: This metric calculates the time during which cells remain non-dividing while retaining the ability to form a colony. Chronological aging is analogous to the aging process in non-dividing cells like neurons [12].

Our study revealed a significant increase in reproductive potential in CMG/cmg strains without any adverse effects on the overall lifespan. This suggests a potential parallel in human cells, where the reduced levels of MCM subunits detected in fibroblasts [34] may originate from sources other than transcription levels, such as changes in the half-life of MCM subunits in senescent cells, possibly influenced by post-translational modifications.

Intriguingly, we also observed a substantial delay in chronological aging in the CMG/cmg strains. This implies a connection between the CMG helicase and post-mitotic growth metabolism or the activation of molecular pathways involved in responding to environmental stressors like acetic acid or pH fluctuations.

Our current findings align with previous reports regarding *ORC/orcΔ* heterozygous strains showing delayed aging in both aging models [8]. Thus, it appears that decreased expression levels of genes associated with replication initiation, including subunits of ORC and CMG complexes, play a pivotal role in aging. These genes are not only vital for growth but also require precise regulation in the context of both replication and aging.

From an evolutionary perspective, a cell population's ability to achieve efficient DNA synthesis and rapid doubling times is crucial, providing a competitive advantage in the competition for environmental resources. Here, we reported that when the expression of genes encoding CMG helicase subunits is reduced, the cells exhibit a significant increase in reproductive potential compared to the WT strain while

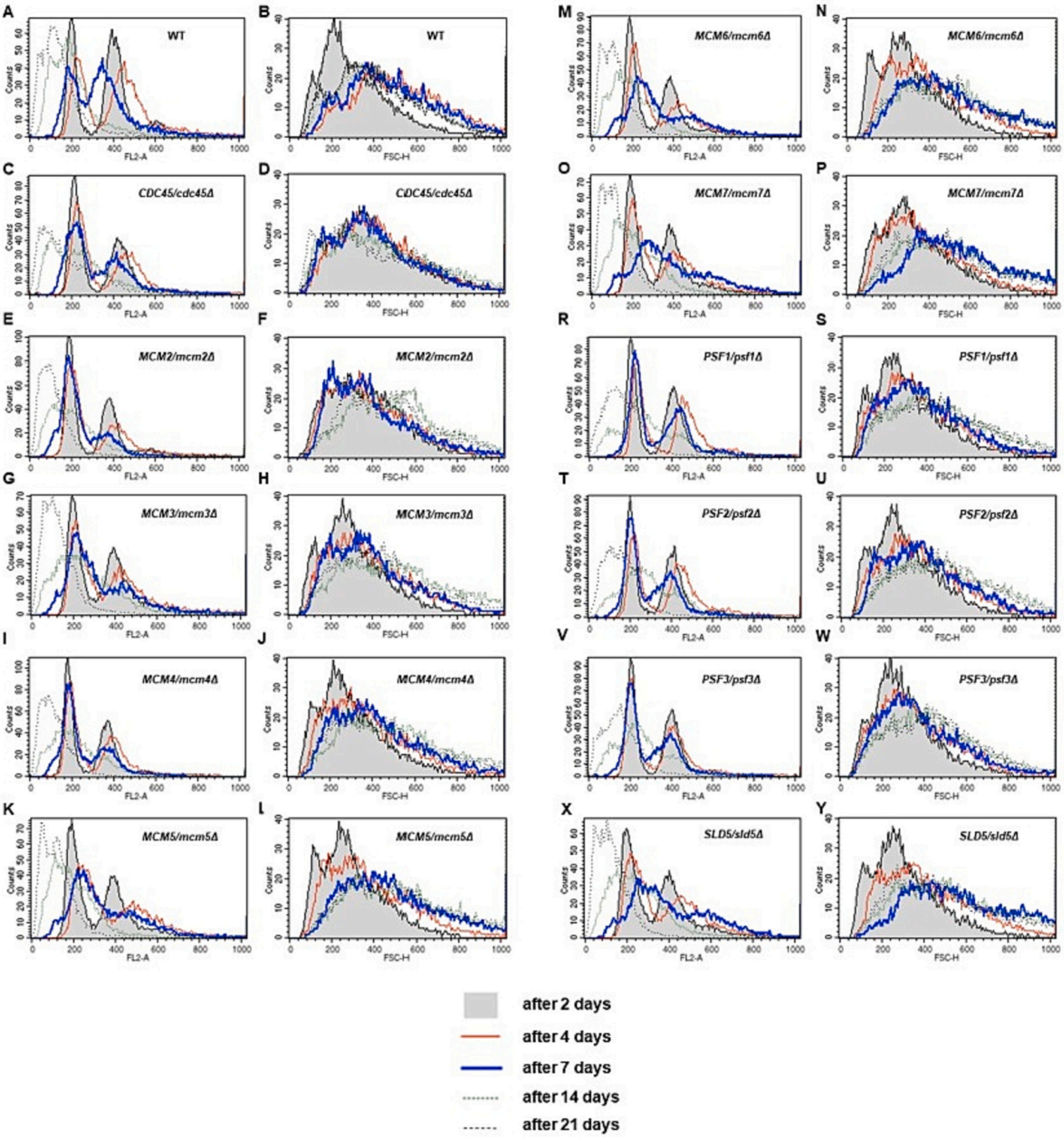

Fig. 7. Ploidy reduction and cell size increase accompany chronological aging. Results of the DNA content analysis by flow cytometry during the chronological aging at 2, 4, 7, 14, and 21 days (A, C, E, G, I, K, M). For the DNA content analysis, yeast cells were stained with propidium iodide (see the Material and Methods section for details). The representative histograms are shown from three independent experiments. Cell size of the diploid control (BY4743) and the isogenic heterozygous strains *CDC45/cdc45Δ*, *MCM2/mcm2Δ*, *MCM3/mcm3Δ*, *MCM4/mcm4Δ, MCM5/mcm5Δ*, *MCM6/mcm6Δ*, *MCM7/mcm7Δ, PSF1/psf1Δ*, *PSF2/psf2Δ*, *PSF3/psf3Δ*, and *SLD5/sld5Δ* during the chronological aging analysis in selected time points (B, D, F, H, J, L, N). The forward scatter (FSC) histograms reflect cell size in the population. Cells were analyzed via flow cytometry as described in the Materials and Methods section. Ten thousand cells per sample were assayed.

simultaneously extending the doubling time. This phenotype bears a resemblance to that of cancer cells.

Among factors contributing to aging, one of the most significant is cell energy metabolism. In our study, we demonstrated that variations in gene copy numbers influence the speed of aging. This is consistent with our previous findings indicating that the overexpression of ribosomal paralogs *uL6A* or *uL6B* accelerates aging in budding yeast [36]. Despite the discovery of many cellular pathways involved in chronological lifespan (CLS) regulation, our understanding of replication initiation during aging remains elusive [8,18].

Intuitively, disturbances in the expression levels of CMG helicase components should not impact post-mitotic aging because chronological aging analysis typically begins at the stationary phase. However, a recent study revealed that over half of the essential yeast genes displayed haploinsufficiency phenotypes under optimal conditions. Furthermore, around 40 % of essential genes, which showed no detectable phenotypes under optimal growth conditions, exhibited haploinsufficiency under stressful conditions [37]. This may explain the

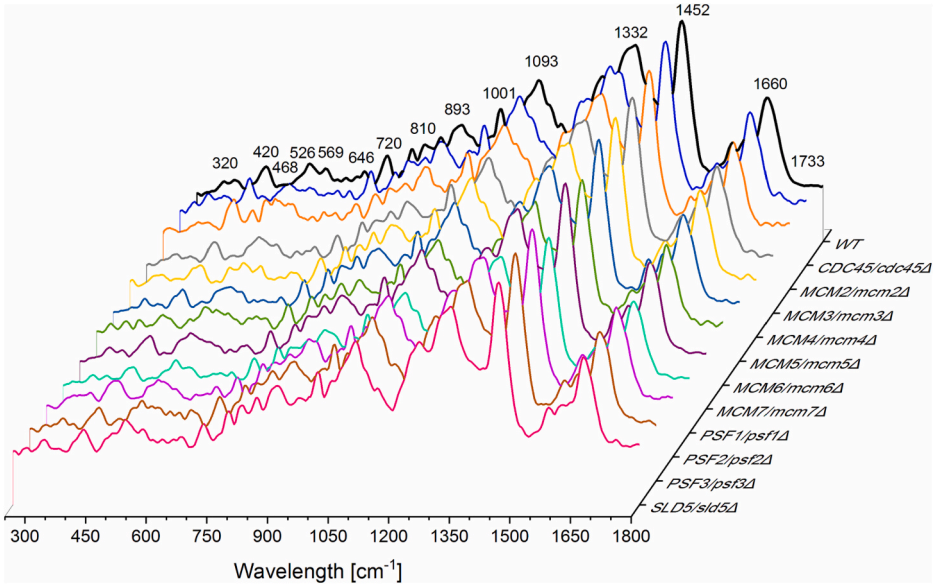

Fig. 8. Raman spectra of the WT control (BY4743) and isogenic heterozygous CMG/cmg strains with marked regions corresponding to vibrations of functional groups for RNA, polysaccharides, proteins, and lipids.

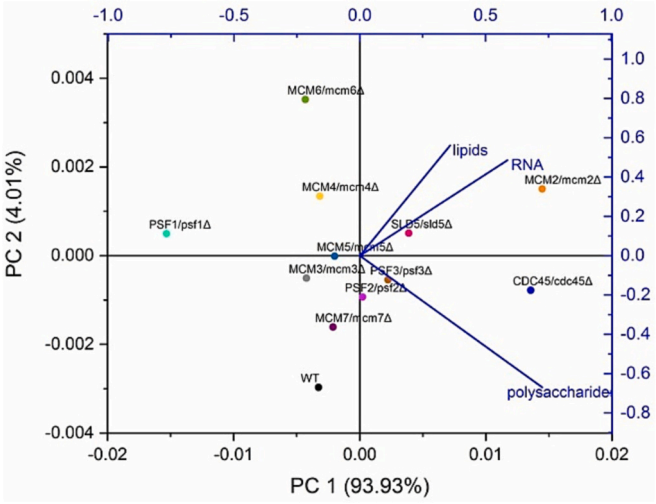

Fig. 9. Results of principal component analysis (PCA) for yeast strains from Raman spectroscopy. PCA presents the relationships between the yeast strains (WT and CMG/cmg strains) and their composition of lipids, polysaccharides, and RNA.

absence of a noticeable phenotype in the *MCM2/mcm2Δ* strain concerning reproductive potential and the significant delay in chronological aging observed in all analyzed heterozygous CMG/cmg strains.

In this regard, CLS can be viewed as a cellular response to stressful conditions, primarily including starvation and acidification of the environment. Our chronological aging analysis confirmed our earlier findings that cells that survive aging increase in size over time [38]. DNA content analysis of chronological aging diploid cells also confirmed previously discovered ploidy changes toward the haploid [8]. In yeast cells, changes in ploidy toward haploidy can be induced by various factors, including single-gene deletions involving important genome stability factors like Rad52 recombinase or replication initiation factor Ctf18 [39,40], extended cultivation [40,41], or starvation [8]. In humans, ploidy shifts are also observed, particularly during DNA damage stress. Improperly repaired DNA damage can lead to aneuploidy, eventually resulting in mitotic catastrophe during subsequent cell division [42]. Chromosome missegregation leading to aneuploidy is often correlated with tumors and likely provides a mechanism for the loss of tumor suppressor genes and the acquisition of extra copies of oncogenes, thus supporting carcinogenesis. It has been reported that approximately 68 % of solid tumors are aneuploid. Notably, chromosome loss is more frequently observed than gain, and smaller chromosomes are lost more frequently than larger ones [43]. Additionally, it has been suggested that ploidy reduction may be an early step in the development of hepatocarcinogenesis from polyploid hepatocytes [44]. Consequently, the ploidy shift reported in this study appears to be a universal phenomenon linked to stressful conditions, subsequent endogenous damage, and cell adaptation to such conditions.

This conclusion is supported by the results of Ravichandran et al., who induced high rates of chromosome missegregation to investigate how yeast cells adapt to chromosome instability over time [45]. Adaptation to chromosome instability occurs through individual chromosomal aneuploidies, resulting in adapted strains with complex karyotypes featuring specific combinations of beneficial chromosomes.

Metabolomics data published by Yosida et al. [46] have suggested a potential association between the biochemical state of yeast cells and their longevity to some extent. In the context of yeast aging, lipid metabolism and homeostasis have been assigned crucial roles [8,16,47]. In our current study, we aimed to investigate whether metabolomic profiles differed between the heterozygous CMG/cmg strains and the WT control.

The data indicated a positive correlation between the content of lipids and RNA, while a strong negative correlation was observed between these components and the content of polysaccharides in the tested strains. Additionally, a robust negative correlation between polysaccharide levels and the reproductive potential of the tested strains was identified. A moderate correlation between RNA levels and the strains' reproductive potential was also evident. Furthermore, we established a significant correlation between the doubling time and the level of fatty acids.

The findings from this study clearly underscore the critical role of the expression levels of genes encoding the CMG complex subunits in yeast metabolism and aging. It is important to note, however, that these observations primarily pertain to replicative aging. So far, our understanding of biochemical changes during chronological aging has been limited. Previous research has indicated that the metabolic profiles of cells lacking Sch9, the major TORC1 effector, differed significantly from

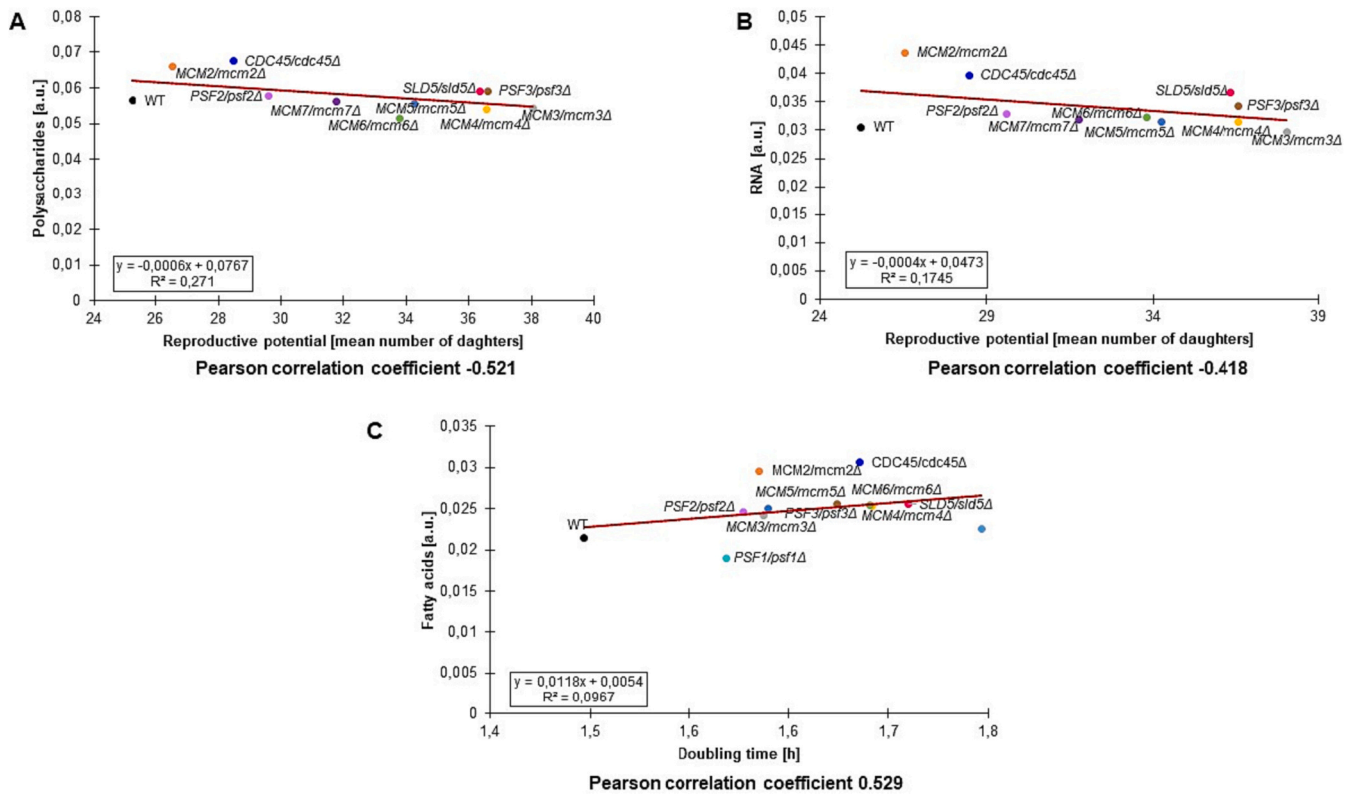

Fig. 10. Relationship between reproductive potential and the polysaccharides level (A), reproductive potential and the RNA level (B) and the doubling time and fatty acids level according to Pearson's correlation coefficient of the WT and the isogenic CMG/cmg strains.

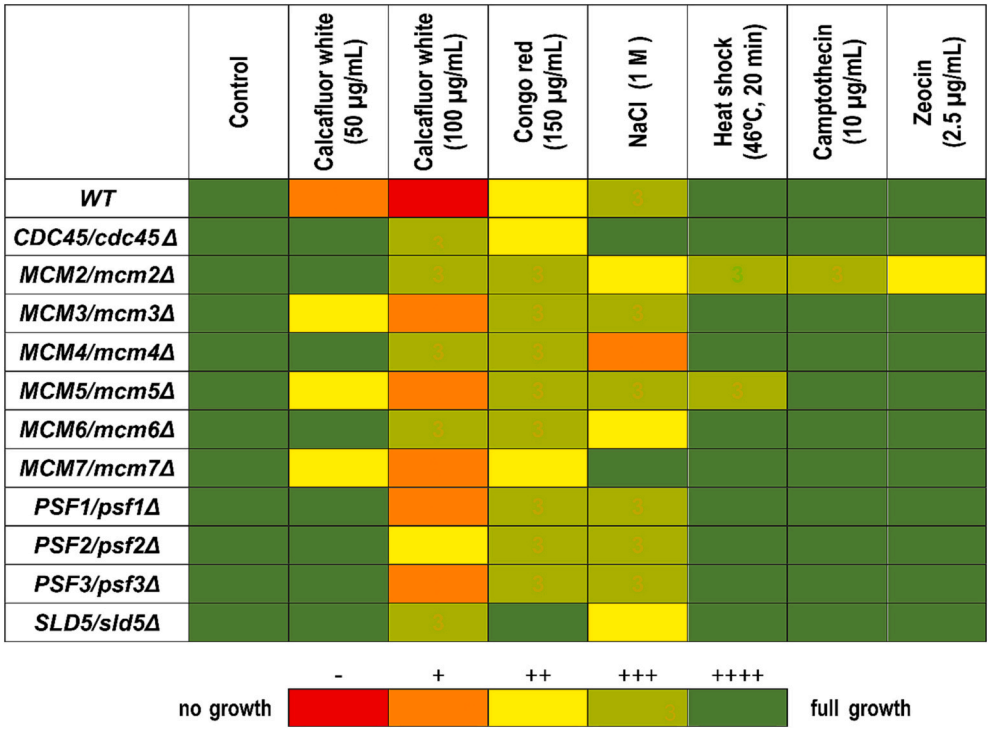

Fig. 11. Heat map representing growth phenotype of heterozygous CMG/cmg yeast strains exposed to different environmental stresses. Strains grown in YPD liquid medium were spotted on YPD medium plates containing the indicated amounts of Calcofluor white, Congo red, sodium chloride (NaCl), zeocin, or camptothecin, then incubated for 2 days at 28 °C. Heat stress was applied by exposition of cells to 46 °C for 20 min. Growth on YPD medium plates served as control. Representative results from two independent experiments are shown. Colors represent the strains' ability to grow in a given condition. Every "+" reflects the growth of colonies on the spot where drops containing 50,000, 5000, 500, and 50 cells, respectively, were placed.

those of wild-type and TOR1-deficient cells. Several antiaging biomarkers have been identified, including intracellular levels of pyruvate, glucose, ribose/deoxyribose-associated compounds, and the presence of specific protein conformational structures. Interestingly, glycogen content increased in the *sch9Δ* strain as aging progressed, whereas it decreased in the wild-type and *tor1Δ* strains [48].

In humans, changes in gene expression, particularly in genes whose products are involved in replication initiation, have been discovered to be associated with various diseases, making them potential targets for treatment. A strong correlation has been observed between the expression of GINS2 (the human equivalent of yeasts' PSF2) and cancer. Notably, a significant increase in GINS2 expression has been reported in various types of cancer, including cervical cancer [49], breast cancer [50], glioma [51], pancreatic cancer [52], and non-small-cell lung cancer [53]. Upregulated GINS2 expression promotes tumor development by enhancing tumor cell proliferation and inhibiting cell apoptosis [52,54]. Recent research has indicated that the CMG complex could be a promising therapeutic target for cancer treatment. Furthermore, small molecule inhibitors of the CMG helicase, such as genistein, metformin, and breviscapine, have been identified as potential anticancer compounds [55–57].

Recent studies have underscored the significance of MCM proteins in the health and well-being of higher eukaryotes. For instance, mice with lower *MCM2* expression levels exhibited a shorter average lifespan due to a higher incidence of cancer, primarily T-cell and B-cell lymphomas [58]. Reduced *MCM2* expression has also been linked to increased levels of Ser139-phosphorylation-induced foci of histone H2AX in muscle cells, which serves as a marker for double-strand DNA breaks. Additionally, MCM expression levels positively correlate with cancer malignancy in several MCM-related cancers, including lung squamous cell carcinoma, renal cell carcinoma, prostate cancer, breast cancer, gastrointestinal tract tumors, brain tumors, and lymphomas (as reviewed in [59]). Furthermore, it has been suggested that MCM2–MCM7 expression levels could serve as prognostic markers for survival in patients with various types of cancer [60].

In conclusion, the progression of the cell cycle is contingent upon the expression levels of essential genes encoding the subunits of the CMG helicase complex. A notable increase in reproductive potential is strongly associated with a reduction in the expression of these genes. However, this reduced gene expression does not impact the overall lifespan of mitotically active cells but rather delays chronological aging. We have also presented additional evidence indicating that diploid cells experience a reduction in ploidy during chronological aging. We postulate that this phenomenon may be linked to the exposure of cells to increasingly stressful conditions over time. Nevertheless, further research is necessary to precisely elucidate the novel mechanism behind this ploidy shift.

Furthermore, our study has revealed a correlation between the levels of RNA or polysaccharides in yeast and their reproductive potential, as well as a relationship between the levels of fatty acids and the doubling time of cells. We have demonstrated that even slight alterations in cell cycle progression resulting from reduced expression of CMG helicase components lead to differences in the biochemical profile of the cells. Importantly, our research sheds new light on the potential use of yeast in investigating potential therapeutic targets for cancer treatment.

CRediT authorship contribution statement

Conceptualization: Mateusz Mołoń, Adrianna Skoneczna.

Methodology: Mateusz Mołoń, Adrianna Skoneczna, Łukasz Jurczyk, Monika Kula-Maximenko Statistical analysis: Karolina Stępień, Mateusz Mołoń.

Investigation: Karolina Stępień, Adrianna Skoneczna, Łukasz Jurczyk, Monika Kula-Maximenko, Mateusz Mołoń.

Writing: Mateusz Mołoń, Karolina Stępień, Adrianna Skoneczna.

Supervision: Mateusz Mołoń.

All authors read and approved the final manuscript.

Declaration of competing interest

The authors declare that they have no known competing financial interests or personal relationships that could have appeared to influence the work reported in this paper.

Data availability

No data was used for the research described in the article.

References

[1] N. Sakakibara, L.M. Kelman, Z. Kelman, Unwinding the structure and function of the archaeal MCM helicase, Mol. Microbiol. 72 (2) (2009) 286–296.
[2] S. Onesti, S.A. MacNeill, Structure and evolutionary origins of the CMG complex, Chromosoma 122 (1–2) (2013) 47–53.
[3] M.E. O'Donnell, H.L. Li, The ring-shaped hexameric helicases that function at DNA replication forks, Nat. Struct. Mol. Biol. 25 (2) (2018) 122–130.
[4] D.R. Reed, M.G. Alexandrow, Myc and the replicative CMG helicase: the creation and destruction of Cancer Myc over-activation of CMG helicases drives tumorigenesis and creates a vulnerability in CMGs for therapeutic intervention, Bioessays 42 (4) (2020).
[5] H. Sedlackova, M.B. Rask, R. Gupta, C. Choudhary, K. Somyajit, J. Lukas, Equilibrium between nascent and parental MCM proteins protects replicating genomes, Nature 587 (7833) (2020), 297−+.
[6] L. Costantino, S.K. Sotiriou, J.K. Rantala, S. Magin, E. Mladenov, T. Helleday, J. E. Haber, G. Iliakis, O.P. Kallioniemi, T.D. Halazonetis, Break-induced replication repair of damaged forks induces genomic duplications in human cells, Science 343 (6166) (2014) 88–91.
[7] J.V. Forment, M.J. O'Connor, Targeting the replication stress response in cancer, Pharmacology & Therapeutics 188 (2018) 155–167.
[8] K. Stepien, A. Skoneczna, M. Kula-Maximenko, L. Jurczyk, M. Molon, Depletion of the origin recognition complex subunits delays aging in budding yeast, Cells 11 (8) (2022).
[9] T.B.L. Kirkwood, S.N. Austad, Why do we age? Nature 408 (6809) (2000) 233–238.
[10] C. Lopez-Otin, M.A. Blasco, L. Partridge, M. Serrano, G. Kroemer, The hallmarks of aging, Cell 153 (6) (2013) 1194–1217.
[11] K.A. Steinkraus, M. Kaeberlein, B.K. Kennedy, Replicative aging in yeast: the means to the end, annual review of cell and developmental biology, annual reviews, Palo Alto (2008) 29–54.
[12] V.D. Longo, G.S. Shadel, M. Kaeberlein, B. Kennedy, Replicative and chronological aging in Saccharomyces cerevisiae, Cell Metab. 16 (1) (2012) 18–31.
[13] M. Molon, M. Szajwaj, M. Tchorzewski, A. Skoczowski, E. Niewiadomska, R. Zadrag-Tecza, The rate of metabolism as a factor determining longevity of the Saccharomyces cerevisiae yeast, Age 38 (1) (2016).
[14] M. Kwolek-Mirek, R. Zadrag-Tecza, Comparison of methods used for assessing the viability and vitality of yeast cells, FEMS Yeast Res. 14 (7) (2014) 1068–1079.
[15] K. Krol, J. Antoniuk-Majchrzak, M. Skoneczny, M. Sienko, J. Jendrysek, I. Rumienczyk, A. Halas, A. Kurlandzka, A. Skoneczna, Lack of G1/S control destabilizes the yeast genome via replication stress-induced DSBs and illegitimate recombination, J. Cell Sci. 131 (24) (2018).
[16] M. Molon, J. Zebrowski, Phylogenetic relationship and Fourier-transform infrared spectroscopy-derived lipid determinants of lifespan parameters in the Saccharomyces cerevisiae yeast, FEMS Yeast Res. 17 (4) (2017).
[17] N. Minois, M. Frajnt, C. Wilson, J.W. Vaupel, Advances in measuring lifespan in the yeast Saccharomyces cerevisiae, Proc. Natl. Acad. Sci. U. S. A. 102 (2) (2005) 402–406.
[18] J. Czachor, M. Milek, S. Galiniak, K. Stepien, M. Dzugan, M. Molon, Coffee extends yeast chronological lifespan through antioxidant properties, Int. J. Mol. Sci. 21 (24) (2020).
[19] A.E. Eastman, S.Q. Guo, The palette of techniques for cell cycle analysis, FEBS Lett. 594 (13) (2020) 2084–2098.
[20] P. Rosch, M. Harz, M. Schmitt, J. Popp, Raman spectroscopic identification of single yeast cells, Journal of Raman Spectroscopy 36 (5) (2005) 377–379.
[21] J.W. Chan, H. Winhold, M.H. Corzett, J.M. Ulloa, M. Cosman, R. Balhorn, T. Huser, Monitoring dynamic protein expression in living E-coli. Bacterial celts by laser tweezers Raman spectroscopy, Cytometry Part A 71A (7) (2007) 468–474.
[22] J. De Gelder, K. De Gussem, P. Vandenabeele, L. Moens, Reference database of Raman spectra of biological molecules, J. Raman Spectrosc. 38 (9) (2007) 1133–1147.
[23] T. Lemma, J. Wang, K. Arstila, V.P. Hytonen, J.J. Toppari, Identifying yeasts using surface enhanced Raman spectroscopy, Spectrochimica Acta Part a-Molecular and Biomolecular Spectroscopy 218 (2019) 299–307.
[24] S.P. Bell, K. Labib, Chromosome duplication in Saccharomyces cerevisiae, Genetics 203 (3) (2016) 1027–1067.
[25] L. Bai, Z.N. Yuan, J.C. Sun, R. Georgescu, M.E. O'Donnell, H.L. Li, Architecture of the Saccharomyces cerevisiae replisome, DNA replication: from old principles to new discoveries 1042 (2017) 207–228.
[26] T.D. Deegan, J.F.X. Diffley, MCM: one ring to rule them all, Curr. Opin. Struct. Biol. 37 (2016) 145–151.

[27] P.M.J. Burgers, T.A. Kunkel, Eukaryotic DNA replication fork, Annual Review of Biochemistry 86 (86) (2017) 417–438.
[28] I. Ilves, T. Petojevic, J.J. Pesavento, M.R. Botchan, Activation of the MCM2-7 helicase by association with Cdc45 and GINS proteins, Mol. Cell 37 (2) (2010) 247–258.
[29] E. Grabowska, U. Wronska, M. Denkiewicz, M. Jaszczur, A. Respondek, M. Alabrudzinska, C. Suski, K. Makiela-Dzbenska, P. Jonczyk, I.J. Fijalkowska, Proper functioning of the GINS complex is important for the fidelity of DNA replication in yeast, Mol. Microbiol. 92 (4) (2014) 659–680.
[30] M. Jedrychowska, M. Denkiewicz-Kruk, M. Alabrudzinska, A. Skoneczna, P. Jonczyk, M. Dmowski, I.J. Fijalkowska, Defects in the GINS complex increase the instability of repetitive sequences via a recombination-dependent mechanism, PLoS Genet. 15 (12) (2019).
[31] S.A. MacNeill, Structure and function of the GINS complex, a key component of the eukaryotic replisome, Biochem. J. 425 (2010) 489–500.
[32] P. Zegerman, Evolutionary conservation of the CDK targets in eukaryotic DNA replication initiation, Chromosoma 124 (3) (2015) 309–321.
[33] Y. Kamimura, Y.S. Tak, A. Sugino, H. Araki, Sld3, which interacts with Cdc45 (Sld4), functions for chromosomal DNA replication in Saccharomyces cerevisiae, EMBO J. 20 (8) (2001) 2097–2107.
[34] Y. Suzuki, Y. Yamaguchi, H. Hanada, Y. Ishimi, Changes in MCM2-7 proteins at senescence, Genes Genet. Syst. 94 (3) (2019) 123–132.
[35] J. Flach, S.T. Bakker, M. Mohrin, P.C. Conroy, E.M. Pietras, D. Reynaud, S. Alvarez, M.E. Diolaiti, F. Ugarte, E.C. Forsberg, M.M. Le Beau, B.A. Stohr, J. Mendez, C. G. Morrison, E. Passegue, Replication stress is a potent driver of functional decline in ageing haematopoietic stem cells, Nature 512 (7513) (2014), 198−+.
[36] M. Molon, M. Zaciura, D. Wojdyla, E. Molestak, Increasing the number of ribosomal uL6 mRNA copies accelerates aging of the budding yeast, Mol. Biol. Rep.
[37] S. Ohnuki, Y. Ohya, High-dimensional single-cell phenotyping reveals extensive haploinsufficiency, PLoS Biol. 16 (5) (2018).
[38] K. Stepien, D. Wojdyla, K. Nowak, M. Molon, Impact of curcumin on replicative and chronological aging in the Saccharomyces cerevisiae yeast, Biogerontology 21 (1) (2020) 109–123.
[39] K. Krol, I. Brozda, M. Skoneczny, M. Bretne, A. Skoneczna, A genomic screen revealing the importance of vesicular trafficking pathways in genome maintenance and protection against genotoxic stress in diploid Saccharomyces cerevisiae cells, PloS One 10 (3) (2015).
[40] W. Song, T.D. Petes, Haploidization in Saccharomyces cerevisiae induced by a deficiency in homologous recombination, Genetics 191 (1) (2012) 279–284.
[41] A.C. Gerstein, R.M. McBride, S.P. Otto, Ploidy reduction in Saccharomyces cerevisiae, Biol. Lett. 4 (1) (2008) 91–94.
[42] I. Vitale, L. Galluzzi, M. Castedo, G. Kroemer, Mitotic catastrophe: a mechanism for avoiding genomic instability, Nat. Rev. Mol. Cell Biol. 12 (6) (2011) 384–391.
[43] P.H.G. Duijf, N. Schultz, R. Benezra, Cancer cells preferentially lose small chromosomes, Int. J. Cancer 132 (10) (2013) 2316–2326.
[44] T. Matsumoto, L. Wakefield, A. Peters, M. Peto, P. Spellman, M. Grompe, Proliferative polyploid cells give rise to tumors via ploidy reduction, Nat. Commun. 12 (1) (2021).
[45] M.C. Ravichandran, S. Fink, M.N. Clarke, F.C. Hofer, C.S. Campbell, Genetic interactions between specific chromosome copy number alterations dictate complex aneuploidy patterns, Genes Dev. 32 (23–24) (2018) 1485–1498.
[46] R. Yoshida, T. Tamura, C. Takaoka, K. Harada, A. Kobayashi, Y. Mukai, E. Fukusaki, Metabolomics-based systematic prediction of yeast lifespan and its application for semi-rational screening of ageing-related mutants, Aging Cell 9 (4) (2010) 616–625.
[47] J. Petschnigg, H. Wolinski, D. Kolb, G. Zellnig, C.F. Kurat, K. Natter, S.D. Kohlwein, Good fat, essential cellular requirements for triacylglycerol synthesis to maintain membrane homeostasis in yeast, Journal of Biological Chemistry 284 (45) (2009) 30981–30993.
[48] M. Bermudez-Moretti, J.F. Gulias, J. Valencia-Guillen, S.A. Munoz, I. Forfar, S. Correa-Garcia, Monitoring changes in the cellular content of biomolecules during ageing with FTIR spectroscopy, Vibrational Spectroscopy 105 (2019).
[49] F. Ouyang, J.L. Liu, M. Xia, C.Y. Lin, X.Q. Wu, L.P. Ye, L.B. Song, J. Li, J. Wang, P. Guo, M. He, GINS2 is a novel prognostic biomarker and promotes tumor progression in early-stage cervical cancer (vol 37, pg 2652, 2017), Oncol. Rep. 45 (5) (2021).
[50] P. Liang, Z.G. Song, D.M. Chen, R.X. Linghu, Y.Z. Wang, X.Y. Zhang, X.X. Kou, J. L. Yang, S.C. Jiao, GINS2 regulates matrix metallopeptidase 9 expression and cancer stem cell property in human triple negative breast cancer, Biomed. Pharmacother. 84 (2016) 1568–1574.
[51] Y.L. Shen, H.Z. Li, Y.W. Hu, L. Zheng, Q. Wang, Loss of GINS2 inhibits cell proliferation and tumorigenesis in human gliomas, CNS Neurosci. Ther. 25 (2) (2019) 273–287.
[52] F.Q. Bu, X.J. Zhu, X. Yi, C. Luo, K. Lin, J.F. Zhu, C.G. Hu, Z.T. Liu, J.F. Zhao, C. Huang, W.J. Zhang, J. Huang, Expression profile of GINS complex predicts the prognosis of pancreatic cancer patients, Onco. Targets. Ther. 13 (2020) 11433–11444.
[53] F. Chi, Z. Wang, Y.Z. Li, N. Chang, Knockdown of GINS2 inhibits proliferation and promotes apoptosis through the p53/GADD45A pathway in non-small-cell lung cancer, Bioscience Reports 40 (2020).
[54] Y. Ye, Y.N. Song, S.F. He, J.H. Zhuang, G.Y. Wang, W. Xia, GINS2 promotes cell proliferation and inhibits cell apoptosis in thyroid cancer by regulating CITED2 and LOXL2, Cancer Gene Ther. 26 (3–4) (2019) 103–113.
[55] S. Majid, A.A. Dar, S. Saini, Y. Chen, V. Shahryari, J. Liu, M.S. Zaman, H. Hirata, S. Yamamura, K. Ueno, Y. Tanaka, R. Dahiya, Regulation of Minichromosome maintenance gene family by MicroRNA-1296 and Genistein in prostate Cancer, Cancer Res. 70 (7) (2010) 2809–2818.
[56] S.H. Kim, S.C. Kim, J.L. Ku, Metformin increases chemo-sensitivity via gene downregulation encoding DNA replication proteins in 5-Fu resistant colorectal cancer cells, Oncotarget 8 (34) (2017) 56546–56557.
[57] Y.B. Guan, D.R. Yang, S.J. Nong, J. Ni, C.H. Hu, J. Li, J. Zhu, Y.X. Shan, Breviscapine (BVP) inhibits prostate cancer progression through damaging DNA by minichromosome maintenance protein-7 (MCM-7) modulation, Biomed. Pharmacother. 93 (2017) 103–116.
[58] S.C. Pruitt, K.J. Bailey, A. Freeland, Reduced Mcm2 expression results in severe stem/progenitor cell deficiency and cancer, Stem Cells 25 (12) (2007) 3121–3132.
[59] S. Yu, G.Q. Wang, Y. Shi, H.F. Xu, Y.C. Zheng, Y. Chen, MCMs in cancer: prognostic potential and mechanisms, Analytical Cellular Pathology 2020 (2020).
[60] S. Schimmack, B. Lawrence, B. Kenney, H. Schmitz-Winnenthal, I.M. Modlin, M. Kidd, Minichromosome maintenance expression defines slow-growing Gastroenteropancreatic neuroendocrine neoplasms, Transl. Oncol. 9 (5) (2016) 411–418.
[61] T. Enkhbaatar, M. Skoneczny, K. Stępień, M. Mołoń, A. Skoneczna, Live while the DNA lasts. The role of autophagy in DNA loss and survival of diploid yeast cells during chronological aging Aging (Albany NY). 15: doi:10.18632/aging.205102.